

SPH MODELING OF RAPID MULTIPHASE FLOWS AND SHOCK WAVE PROPAGATION

Sauro Manenti¹, Stefano Sibilla¹, Mario Gallati¹, Giordano Agate², Roberto Guandalini²

¹ University of Pavia, Dept. Of Hydraulic and Environmental Eng.
via Ferrata, 1 27100 Pavia (Italy)
e-mail: {sauro.manenti, stefano.sibilla, gallati}@unipv.it

² Environment and Sustainable Development Dept., RSE s.p.a.
Via Rubattino, 54 – 20134 Milan, Italy
{giordano.agate, roberto.guandalini}@rse-web.it

Keywords: Smoothed Particle Hydrodynamics, non-cohesive sediment, reservoir flushing, underwater explosion, experimental validation.

Abstract. *This work shows an application of the Smoothed Particle Hydrodynamics (SPH) for the numerical modeling of engineering problems involving rapid evolution over time, high strain and gradients, heterogeneity, deformable contours and the presence of mobile material interfaces.*

Following a Lagrangian approach the continuum is discretized by means of a finite number of material particles carrying physical properties and moving according to Newton's equations of the classical physics. Spatial derivatives of a variable at a point are approximated by using the information on the neighboring particles based on the kernel approximation.

This paper recalls the basics of the method along with some numerical aspects concerning boundaries treatment, time integration scheme etc.; furthermore some details are provided about the recent improvements carried out for SPH simulations of: a) non-cohesive sediment flushing by rapid water discharge in an hydropower reservoir, b) underwater explosion for bottom sediment resuspension in an artificial reservoir.

Numerical examples are illustrated and discussed concerning 2D and 3D test cases carried out with the aim of investigating the basic features of both sediment dynamics and gas explosion: obtained results shows that the SPH method can be applied to model the relevant engineering aspects of the considered problems and can be a helpful tool for future design applications in the field of hydropower reservoir management.

1 INTRODUCTION

The key idea at the base of a meshfree method is to obtain a discretization of the continuum through a set of arbitrarily distributed nodes (or particles) that lack of a connective mesh and can adapt to possible topological and geometrical changes.

With respect to traditional grid-based approaches, a meshless method allows tracing the deformation undergone by the material without excessive degradation of numerical results (owing to conflicts between mesh and physical compatibility) and high computational effort (e.g. adaptive mesh refinement).

When the nodes assumes a physical meaning (i.e. they represent material particles carrying physical properties such as mass, momentum etc.) is said a meshfree particle method and follows, in general, a Lagrangian approach.

Among the different meshfree particle methods the Smoothed Particle Hydrodynamics (SPH) was originally developed as a probabilistic model for simulating astrophysical problems [1, 2]. It was later modified as a deterministic meshfree particle method and applied to continuum solid and fluid mechanics [3, 4] because the kinematics and dynamics of the liquid particles, responding to Newton's Equations of the classical physics, could be described in analogy with the simulation of the collective movement of astrophysical particles at large scale.

According to standard SPH, a continuous physical quantity $A(\mathbf{x})$, defined on the domain Ω as a function of the position vector \mathbf{x} , and its spatial derivatives at the i -th material point are approximated by using the information on the neighboring particles based on the kernel estimate.

This procedure adopts a kernel function $W(r, h)$, which is continuous, non-zero and depends on the modulus of the relative position $r = |\mathbf{x}_i - \mathbf{x}_j|$ of the neighboring j -th particle falling within a circular space (spherical in 3D problems) with radius $2h$, where h is generally referred to as the smoothing length (Fig.1).

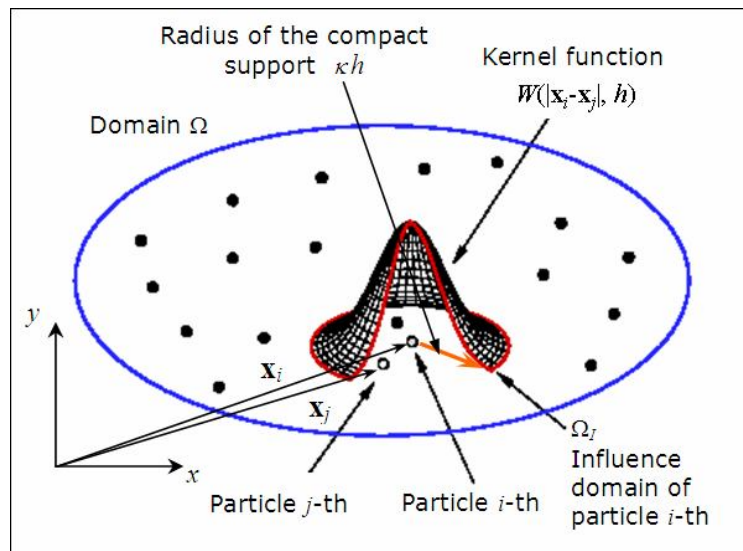


Figure 1: Typical representation of particle discretization and kernel function.

The SPH approximation of the field function $A(\mathbf{x})$ originates from the concept of integral representation:

$$A(\mathbf{x}) = \int_{\Omega} \delta(\mathbf{x} - \mathbf{x}') A(\mathbf{x}') d\Omega_{\mathbf{x}'} \quad (1)$$

In Eq.1 the Dirac delta function δ is replaced by the kernel function leading to the kernel approximation:

$$\langle A(\mathbf{x}) \rangle = \int_{\Omega} W(r, h) A(\mathbf{x}') d\Omega_{\mathbf{x}'} \quad (2)$$

The discrete form of the Eq.2, for the set of material particles representing the discretized continuum, can be obtained by the so called particle approximation:

$$\langle A(\mathbf{x}_i) \rangle = \sum_{j=1}^N \frac{m_j}{\rho_j} A(\mathbf{x}_j) W(r_{ij}, h) \quad (3)$$

The summation in Eq.3 is extended over the N -neighboring particles, having volume $\Delta V_j = m_j / \rho_j$, falling within the compact support (or influence domain) Ω_i of the i -th particle.

In a similar fashion it can be demonstrated that the particle approximation of the function derivative can be obtained by shifting the differential operation on the kernel; two alternative expressions are commonly adopted in fluid mechanics [5, 6]:

$$\begin{aligned} \langle \nabla \cdot A(\mathbf{x}_i) \rangle &= \frac{1}{\rho_i} \sum_{j=1}^N m_j [A(\mathbf{x}_j) - A(\mathbf{x}_i)] \cdot \nabla W(r_{ij}, h) \\ \langle \nabla \cdot A(\mathbf{x}_i) \rangle &= \rho_i \sum_{j=1}^N m_j \left[\frac{A(\mathbf{x}_j)}{\rho_j^2} + \frac{A(\mathbf{x}_i)}{\rho_i^2} \right] \cdot \nabla W(r_{ij}, h) \end{aligned} \quad (4)$$

Applying the SPH interpolation, the Lagrangian form of the Navier-Stokes equations for a weakly compressible viscous fluid can be transformed into a system of ordinary differential equations that, by adopting the equations (4) and replacing $W(r_{ij}, h)$ with W_{ij} , are written as:

$$\begin{aligned} \left\langle \frac{D\rho}{Dt} \right\rangle_i &= - \sum_{j=1}^N m_j (\mathbf{u}_j - \mathbf{u}_i) \cdot \nabla W_{ij} \\ \left\langle \frac{D\mathbf{u}}{Dt} \right\rangle_i &= - \sum_{j=1}^N m_j \left(\frac{p_i}{\rho_i^2} + \frac{p_j}{\rho_j^2} + \Pi_{ij} \right) \nabla W_{ij} + \mathbf{g} \\ &\quad + \sum_{j=1}^{N_i} \frac{m_j}{\rho_i \rho_j} \frac{4 \mu_i \mu_j}{\mu_i + \mu_j} \frac{\mathbf{x}_{ij} \cdot \nabla W_{ij}}{\mathbf{x}_{ij}^2 + 0.01 h^2} \mathbf{u}_{ij} \end{aligned} \quad (5)$$

The additional term Π_{ij} in Eq.5 is the so called Monaghan artificial viscosity [4] introduced for numeric stability:

$$\Pi_{ij} = \begin{cases} \frac{-\alpha_M (c_{s i} + c_{s j})}{\rho_i + \rho_j} \phi_{ij} + \frac{2\beta_M}{\rho_i + \rho_j} \phi_{ij}^2 & \text{if } \mathbf{u}_{ij} \cdot \mathbf{x}_{ij} < 0 \\ 0 & \text{if } \mathbf{u}_{ij} \cdot \mathbf{x}_{ij} > 0 \end{cases} \quad \phi_{ij} = \frac{h \mathbf{u}_{ij} \cdot \mathbf{x}_{ij}}{\mathbf{x}_{ij}^2 + (0.1h)^2} \quad (6)$$

There are several advantages that can be obtained from such an approach: representation of the evolution of both free-surfaces, moving-interfaces and breaking becomes more simple to face with [7]; treatment of large deformation and shock problems becomes a relatively easier task [8]; the particle tracking along with the relevant field variables can be obtained by numerical solution of the discretized set of governing equations in Lagrangian form [9].

2 NUMERICAL ASPECTS

The solution strategy of a meshfree particle method follows a pattern similar to a grid-based method.

The computational domain is divided into a finite number of particles, followed by the numerical discretization of the system of partial differential equations according to the procedure described in the previous section; the resulting ordinary differential equations are solved through any stable time-stepping algorithm [10]: here a first order explicit numerical scheme is used and a cubic spline function is adopted for kernel representation [8].

The obtained velocity field allows one to update the particle position \mathbf{x} and to compute the density field by means of the continuity equation (1); the pressure p_i at each point is then calculated through the equation of state for a weakly compressible fluid and then smoothed out:

$$p_i = p_{0i} + \frac{\varepsilon}{\rho} (\rho_i - \rho_{0i})$$

$$p_i^{smth} = p_i + \mathcal{G}_p \frac{\sum_{j=1}^N (p_j - p_i) \Delta V_j W_{ij}}{\sum_{j=1}^N \Delta V_j W_{ij}} \quad (7)$$

Solid boundaries are treated by means of the semi-analytic technique [8]. Each portion of the solid contour contributing to the mass and momentum equations of the generic i -th particle is replaced by a fluid region extending beyond the boundary and treated as a material continuum with uniform velocity ($\mathbf{u}_b = \mathbf{u}_i$), and hydrostatic pressure distribution (Fig.2).

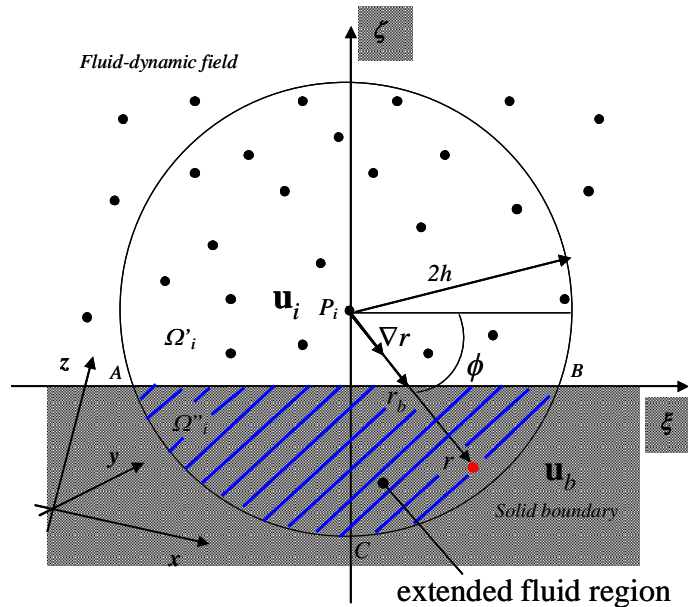


Figure 2: Scheck of boundary treatment (2D case).

A typical term for boundary contribution in the balance equations is:

$$C_1 \int_{\alpha} C_2 J_n(\vartheta, \varphi) d\alpha \quad (8)$$

with: $C_1 = f(\rho_i, \mathbf{u}_i, \mathbf{u}_b, \nu)$ $C_2 = f(\nabla r)$ $J_n(\vartheta, \varphi) = \int_{r_b(\vartheta, \varphi)}^{2h} \frac{dW}{dr} r^n dr$

In Eq.8 $\alpha = f(\vartheta, \varphi)$ denotes the solid angle under which the i -th particle sees the portion of the solid boundary intersected by its sphere of influence and the integrals J_n ($n=1, 2, 3$) depends on the boundary's geometry and can be computed analytically.

3 MODELING NON-COHESIVE SEDIMENT FLUSHING

This Section illustrates some details concerning the SPH modeling of fluid-sediment coupled dynamics in flushing problems induced by rapidly varied water flows.

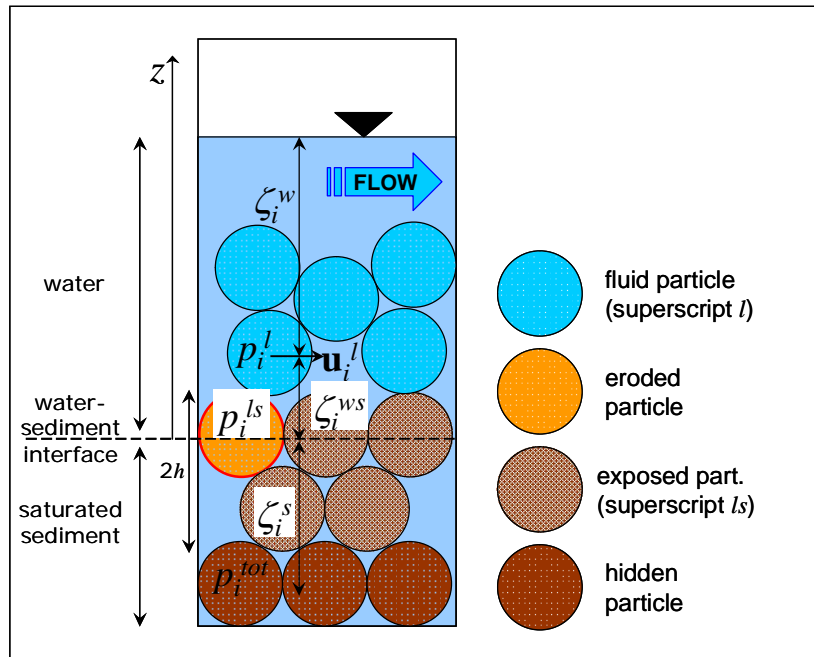


Figure 3: Sketch of the bottom sediment.

In a typical situation schematized by Fig.3, the solid grains can be: *a*) at or very close to the fluid-sediment interface and thus exposed to the hydrodynamic bottom shear or *b*) hidden by the overlaying solid particles.

3.1 Exposed grains

In the first condition the erosion of a single grain is evaluated by means of a failure criterion which is based on the Shields theory and defines a critical threshold that triggers the motion of the solid particle.

The critical bottom shear for an horizontal bed $\tau_{b\ cr,0}$ is evaluated through the Shields parameter \mathcal{G}_{cr} which can be computed as a function of the grain Reynolds number Re_* :

$$\mathcal{G}_{cr} \equiv \frac{\tau_{b\ cr,0}}{(\rho^s - \rho) g d} = f(Re_* \equiv u_* d_{50} / \nu) \quad (9)$$

The erosion of the grain occurs only if the critical bottom shear is exceeded by the hydrodynamic bottom shear:

$$\tau_b = \rho u_*^2 \quad (10)$$

From equations (9) and (10) follows that the friction velocity u_* should be evaluated for determining particle erosion: this is obtained from the computed fluid velocity u^l at a given position z close to the water-sediment interface and assuming a logarithmic velocity profile:

$$u^l(z) = \frac{u_*}{\kappa} \ln\left(\frac{z}{z_0}\right) \quad (11)$$

An iterative procedure should be applied since the characteristic bed roughness z_0 is a function of the friction velocity in turn.

Additional corrective coefficients should be introduced in order to account for a reduction of $\tau_{b\ cr,0}$ owing to both longitudinal and transverse bed slope [11].

If a solid particle is eroded it is considered as a viscous fluid whose kinematics and dynamics responds to the governing equations (5); elsewhere is treated as explained in the following point.

3.2 Hidden grains

In the second condition granular particles are treated as part of the boundary and excluded from the computation of the velocity and density fields; their total pressure (p_i^{tot}) is imposed according to the lithostatic condition and then included in the pressure smoothing of the fluid particles:

$$\begin{aligned} p_i^{ls} &= \zeta_i^{ws} g \rho + p_i^l + \frac{(u_i^l)^2}{2} \rho \\ p_i^{tot} &= p_i^{ls} + \zeta_i^s g \rho^s \end{aligned} \quad (13)$$

Equations (13) imply that the total pressure at the i -th particle inside the solid matrix can be evaluated only if ζ_i^s and ζ_i^{ws} are known: this means that the local fluid-sediment interface needs to be identified at each time step. Such task is accomplished, with a relatively reduced effort, within the algorithm for the neighboring particle search: the spatial domain is divided into squared columns with base length of $2h$ and, for each column, the highest solid and the lowest fluid particles are stored and adopted for imposing the total lithostatic pressure at every time step.

4 MODELING GAS EXPLOSION

The explosion process of a high explosive (HE) material is characterized by a violent oxidation involving a chemical compound and an oxidizer; since the internal energy of the products is lower than the one of the reactants, a great amount of heat (say reaction heat) is quickly released [12].

Even if such a phenomenon develops at very high speed of reaction, in the early phase it is characterized by two distinct inhomogeneous zones: a detonation-produced explosive gas and a non-oxidized explosive; between them a very thin layer exists which represents the front of a reacting shock wave (detonation wave) advancing with a characteristic velocity U .

Anyway in several applications the detonation speed can be assumed indefinitely high and the HE charge completely transformed into gaseous products; their expansion can be analyzed by considering the Euler equation for an inviscid fluid and assuming adiabatic process [6, 13].

As a result the viscous contribution at the right hand side of the linear momentum Eq.5 is neglected, and a balance equation for the gas internal energy is introduced:

$$\left\langle \frac{De}{Dt} \right\rangle_i = \frac{1}{2} \sum_{j=1}^N m_j \left(\frac{p_i}{\rho_i^2} + \frac{p_j}{\rho_j^2} + \Pi_{ij} \right) (\mathbf{u}_i - \mathbf{u}_j) \cdot \nabla W_{ij} \quad (14)$$

The state equation given by eq.15 is used for adiabatic transformation.

$$p_i = (\gamma - 1) \rho_i e_i \quad (15)$$

The kernel function adopted in subsequent analyses is a quintic spline [14], while the time integration is carried out through an explicit numerical scheme deriving from the symplectic algorithm [15].

5 NUMERICAL EXAMPLES

This section provides some numerical results concerning basic SPH simulations of both sediment flushing and gas explosion; the models previously described are adopted.

5.1 Sediment flushing

In the following are illustrated 2D and 3D numerical simulations of non-cohesive sediment flushing by a rapid water flow.

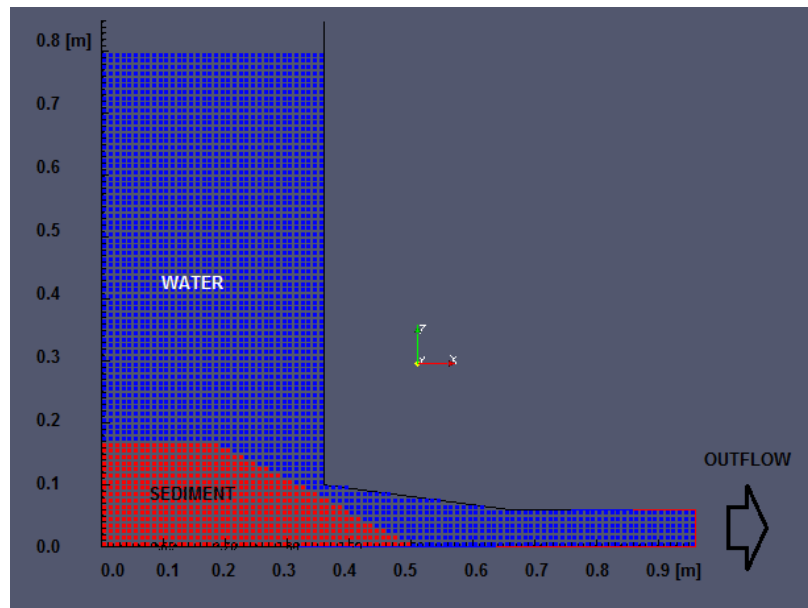


Figure 4: Longitudinal cross-section of the sediment flushing model.

The problem set up is schematized in Fig.4: it simplifies a more refined laboratory test [16] for the analysis of sediment erosion at the midsection of a long-narrow artificial reservoir induced by the opening of the bottom outlet for siltation control.

In order to moderate the computational time, the volume of both sediment and stored water has been lowered by reducing the longitudinal length of the tank toward its left-hand boundary; at the initial time the same water level as in the abovementioned experiment has been assumed, thus keeping the hydraulic head invariant.

The horizontal deposit of non-cohesive sediment is composed of uniform sand with median diameter $d_{50}=0.1$ mm, bed porosity $n=0.53$ and saturated unit volume density $\rho^s=1750$ kg/m³.

The longitudinal measures of the SPH model are shown in Fig.4; the transverse thickness of the 3D model is equal to 0.03m; the resulting total particles number (water plus sediment)

is 3300 and 9900 respectively in the 2D and 3D geometry (transverse thickness equal to 0.03 m); other relevant physical and numerical model parameters are summarized in Tab.1.

MODEL PARAMETERS		
h_0	interpart. distance	0.01 m
h	smoothing length	$1.25 h_0$
ρ_0	water ref. density	1000 kg/m^3
ρ^s	sediment ref. density	1750 kg/m^3
μ	water viscosity	$1.0\text{E-}3 \text{ Pa/s}$
μ^s	sediment viscosity	750 Pa/s
ε	water comp. modulus	$1.0\text{E-}6 \text{ kg/(m s}^2\text{)}$
ε^s	sediment comp. mod.	$1.75\text{E-}6 \text{ kg/(m s}^2\text{)}$
α_M	artificial viscosity	0.2
β_M	artificial viscosity	0.0
\mathcal{G}_p	pressure smoothing	0.2
d_{50}	median grain diameter	$1.0\text{E-}4 \text{ m}$
k_s	char. grain roughness	$3.0 d_{50}$

Table 1: Principal model parameters adopted for flushing computations.

At the initial time the sediment bed has a vertical thickness of 0.165 m; the water height is 0.8 m and it is discharged from the lower right-hand side of the tank at a constant flow rate of $q_0 = 7.9\text{E-}3 \text{ m}^3/\text{s}$ producing the scouring of the bottom sediment.

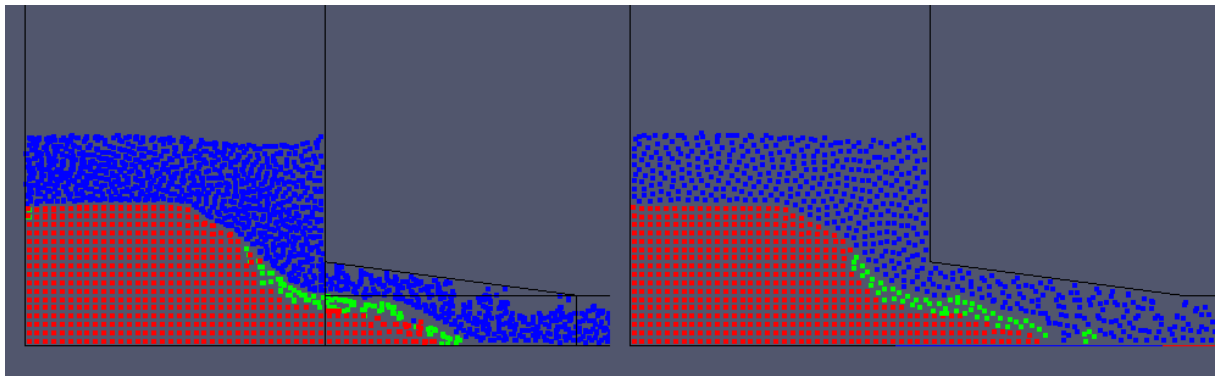


Figure 5: Comparison of eroded profile in 3D (left-hand) and 2D geometry at $t = 11.0 \text{ s}$.

Fig.5 shows a comparison of the eroded sediment profiles at time 11s; water particles are depicted in blue while the color of solid grains depends on their status: the red indicates fixed particles (both hidden and exposed) that are treated as a solid boundary and excluded from the computation, while the green color denotes eroded sediment transported as bed load; the latter are located in that zone where the velocity reaches the highest values (see Fig.6) and are confined within a distance of $2h$ from the water-sediment interface.

From Fig.5 can be seen a good qualitative agreement between 3D and 2D model: similar water free surface and eroded profile are obtained; in both cases the sediment slope is characterized by the presence of a sub-horizontal berm past the intake: this is consistent with

the velocity profile along the flow path during the transient phase and is confirmed by the experimental test during the early phase.

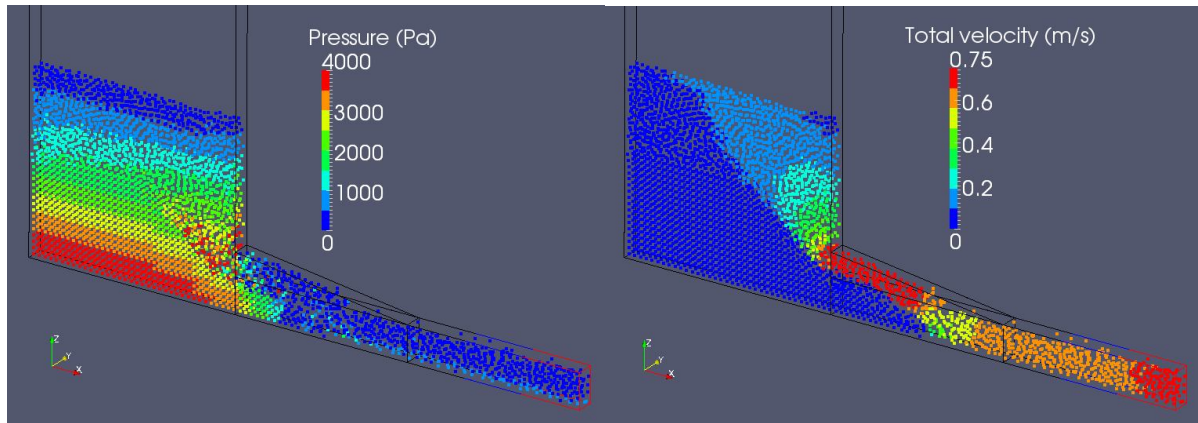


Figure 6: Pressure (left-hand) and velocity profile in 3D model.

Figure 6 displays pressure and velocity profiles obtained with the 3D geometry at $t = 9.00$ s: lithostatic pressure distribution in the fixed solid particles is visible; the velocity modulus is maximum around the intake.

5.2 Gas explosion

In the following are shown some numerical simulations of the expansion process of a HE gas; both the underwater and vacuum expansion of a circular-shaped charge are considered. As previously specified the detonation velocity U is assumed to be indefinitely high with respect to the gas kinematic: thus the explosive charge is assumed completely detonated.

Table 2 summarizes the relevant model parameters adopted in subsequent computations.

MODEL PARAMETERS		
h_0	interpart. distance	0.005 m
h	smoothing length	$1.3 h_0$
ρ_0	water ref. density	1000 kg/m^3
ρ_0^g	gas ref. density	1630 kg/m^3
e_0	spec. detonation energy	$4.29\text{E}+06 \text{ J/kg}$
c_s	speed of sound	$5.0\text{E}+4 \text{ m/s}$
α_M	artificial viscosity	0.2
β_M	artificial viscosity	10.0
\mathcal{D}_v	velocity smoothing	0.2
γ_W	water state equation	1.4 – 7.0
γ_G	gas state equation	1.4

Table 2: Principal model parameters adopted for gas explosion computations.

When considering the vacuum gas expansion, at the initial time 20 particles are placed in the radial direction while 60 particles are positioned along the tangential direction resulting in a total number of 1200. The particle position, velocity and pressure are depicted in Fig.7 at time intervals of $10\mu\text{s}$; axes labels are in meters.

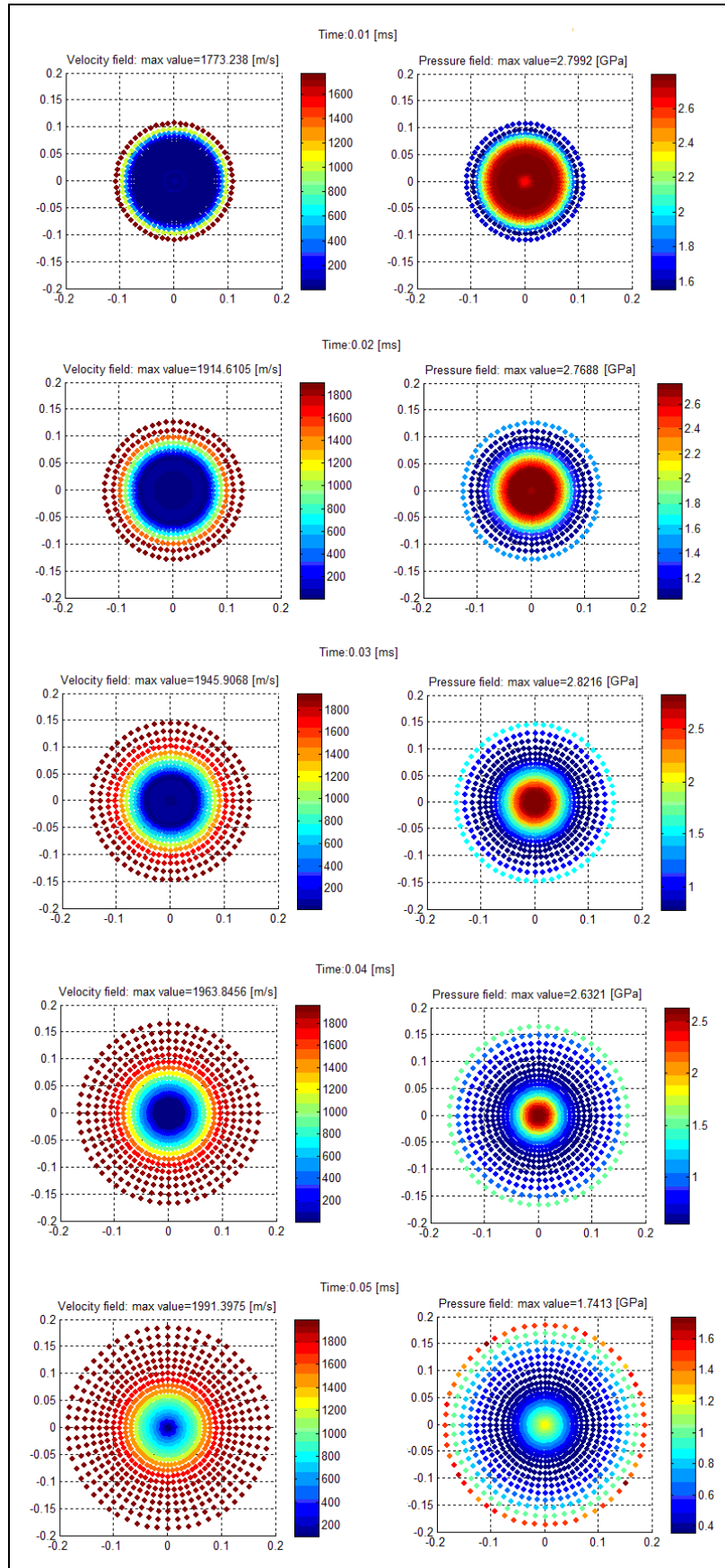


Figure 7: Expansion of detonated gas in vacuum; axes scale in meters.

The charge centre represents a singular point since no particle is placed on it and this explains the lower pressure.

The expansion process reflects theoretical expectation until $t=40\mu\text{s}$: past that time some irregularities in the pressure distribution at the outer boundary of the gaseous mass appear; such a fact should be connected with the lack of information owing to the low number of neighbors in the interaction domain of external particles.

Such non-physical behavior is however avoided if a surrounding medium is considered for confinement of the explosive charge.

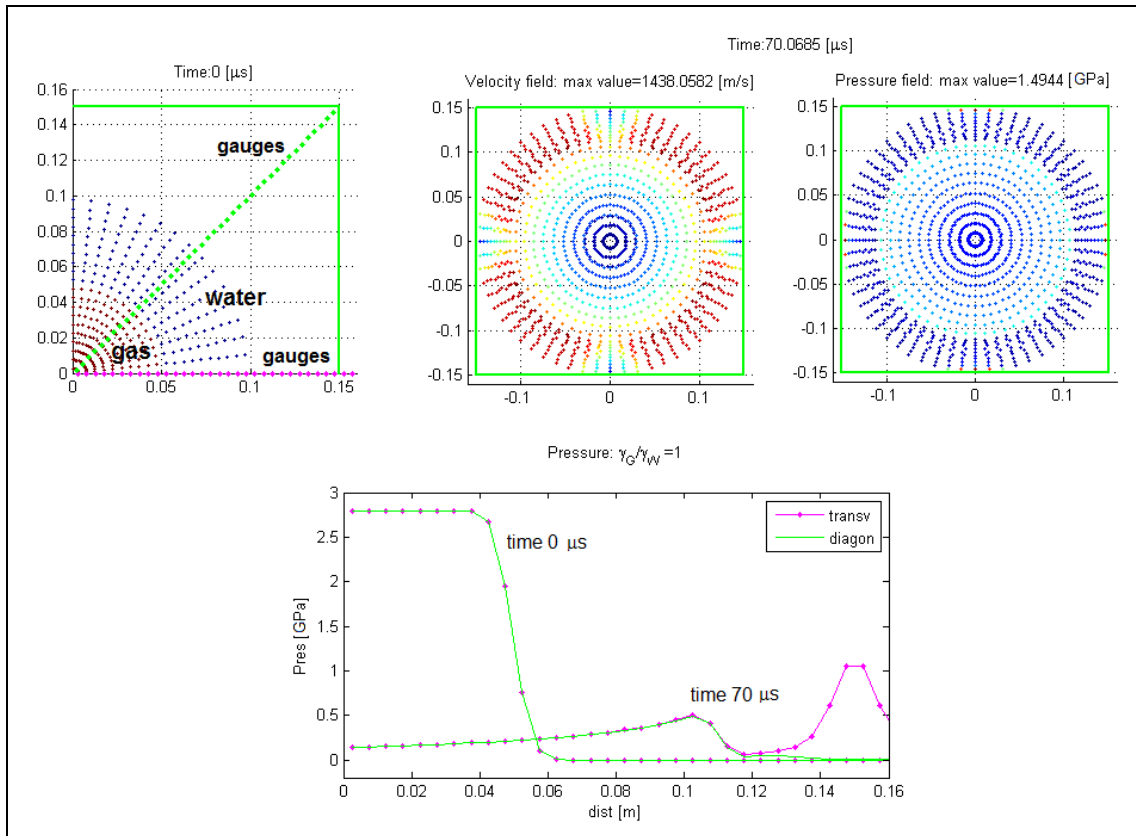


Figure 8: Expansion of detonated gas surrounded by a water crown into a rigid box; axes scale in meters.

Fig.8 shows the expansion of a circular charge surrounded by a water crown and confined in a rigid squared box with length of 0.30 m; the simulation is carried out considering the same compressibility modulus for both gas and water (i.e. $\gamma_G/\gamma_W = 1$).

The upper left-hand panel displays the initial configuration and the position of the gauges for pressure detection on the transversal and diagonal directions; continuous green line denotes the rigid box contour.

The central and right-hand upper panels show particles position, velocity modulus and pressure at time $t = 0.07$ ms when the water impacts with the box walls.

The lower panel shows pressure distribution at initial time ($t = 0.0$ ms) and at the impact time ($t = 0.07$ ms): in the latter a pressure wave is reflected by the box wall and propagates backward along the transversal direction with a peak of about 1 GPa.

The simulation ends at 0.2 ms: after the gas and water particles have completely expand occupying the whole box internal volume, symmetrical jets originates from both transversal and diagonal directions thus pumping the gas toward the box center and producing a contraction of its volume.

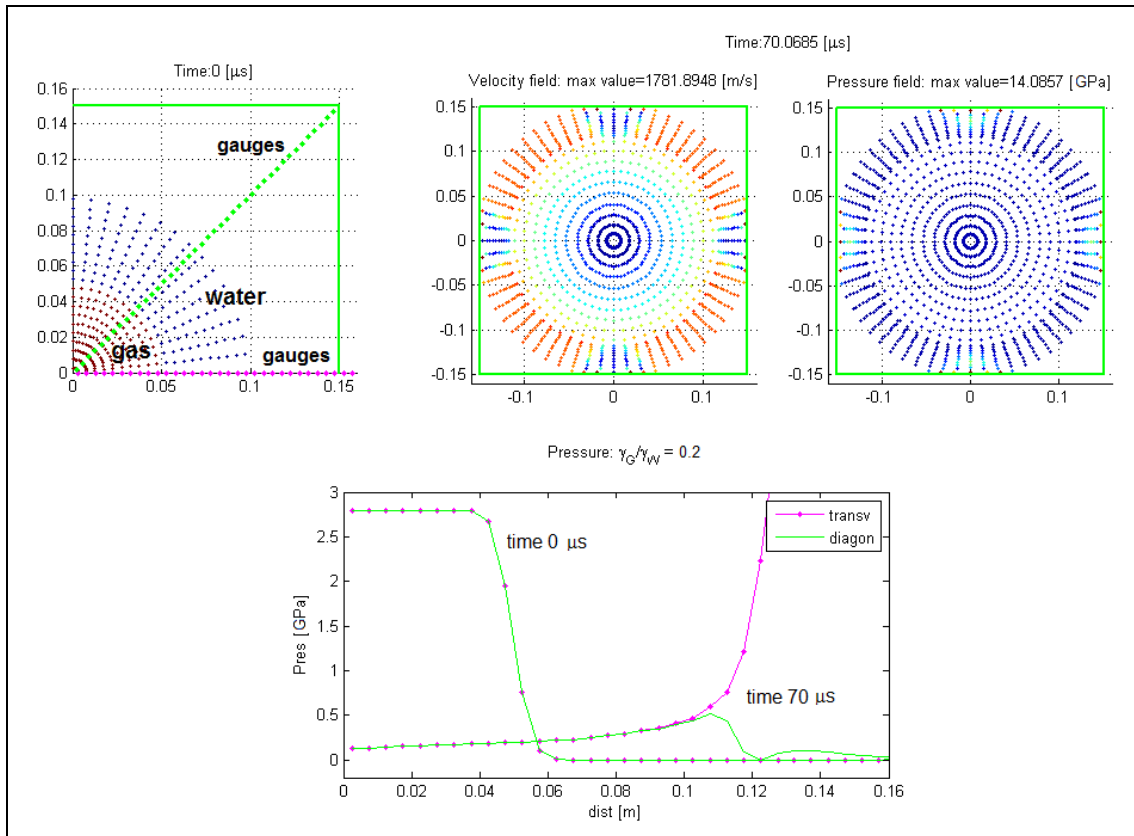


Figure 9: Expansion of detonated gas surrounded by a water crown into a rigid box; axes scale in meters.

Fig.9 shows the results obtained when increasing to 7.0 the value of the gamma water constant in the state equation (i.e. $\gamma_G/\gamma_W=0.2$).

The particles dynamics is rather similar to that one described in the case $\gamma_G/\gamma_W=1$: anyway now the water compressibility modulus is greater than the gas and this produces reflected pressure waves with higher peaks and celerity; the pulsation frequency of the gas expansion and contraction described in the previous analysis is also increased.

6 CONCLUSIONS

An advanced application of the Smoothed Particle Hydrodynamics method for the numerical modeling of rapid multiphase flow and underwater explosion problems have been illustrated in this paper.

The basic features of the numerical model adopted for simulating both non-cohesive sediment flushing and underwater expansion of a HE gas have been illustrated.

The proposed results have shown that the physics of the investigated problems can be simulated with an adequate degree of accuracy for engineering applications.

7 ACKNOWLEDGMENTS

This work has been financed by the Research Fund for the Italian Electrical System under the Contract Agreement between RSE (formerly known as ERSE) and the Ministry of Economic Development - General Directorate for Nuclear Energy, Renewable Energy and Energy Efficiency stipulated on July 29, 2009 in compliance with the Decree of March 19, 2009.

8 LIST OF SYMBOLS

A	physical field function (scalar or vector)
C_n	normalization factor for kernel functions
c_s	speed of sound
d_{50}	median sediment diameter
D/Dt	material derivative
e	internal energy
k_s	characteristic grain roughness height
h	smoothing length
h_0	initial interparticle distance
ΔV	particle volume
m	mass
n	dimension of the physical space
N	neighboring particles
p	pressure
p_0	reference pressure
$r_{ij}= \mathbf{x}_i-\mathbf{x}_j $	modulus of the relative distance vector
u^*	friction velocity
U	detonation wave characteristic velocity
∇r	radial unit vector
\mathbf{g}	gravitational acceleration vector
\mathbf{u}	velocity vector
\mathbf{u}_{ij}	relative velocity vector
\mathbf{u}_b	velocity vector of the solid boundary
\mathbf{x}	position vector
\mathbf{x}_{ij}	relative position vector
dV	elementary volume
α_M, β_M	constants of Monaghan artificial viscosity
δ	<i>Dirac</i> delta function
γ	state equation parameter
ε	fluid compressibility modulus
κ	Von Kàrmàn constant
φ, ϑ, r	spherical coordinates
μ	dynamic viscosity
ν	cinematic viscosity
Π	Monaghan artificial viscosity
ρ	density
ρ^s	sediment density
ρ^g	gas density
ρ_0	reference density
\mathcal{G}_{cr}	Shields parameter
θ_p	pressure smoothing coefficient
$\tau_{b\ cr,0}$	critical bottom shear stress (horizontal bed)
τ_b	hydrodynamic bottom shear
ζ^s	solid particle distance from the water-sediment interface
ζ^w	local draught of the water-sediment interface
ζ^{ws}	fluid particle distance from the water-sediment interface

W	kernel smoothing function
$d\Omega$	elementary volume of the continuum
Ω	spatial domain
Ω_i	compact support (or influence domain) of the i -th particle

REFERENCES

- [1] Lucy L. A numerical approach to the fission hypothesis, *Astron J.*, 82-1013, 1977.
- [2] Gingold R.A., Monaghan J.J. Smoothed particle hydrodynamics: theory and application to non-spherical stars, *Mon Not Roy Astron Soc*, 181-375, 1977.
- [3] Monaghan J.J. Simulating free surface flows with SPH, *J. Comput. Phys.* Vol. 110, 399-406, 1992.
- [4] Monaghan J.J. Smoothed particle hydrodynamics, *Ann. Rev. Astronomy and Astrophysics*, Vol. 30, 543-574, 1992.
- [5] Li S., Liu W.K. *Meshfree Particle Methods*, Springer Ed. 2004.
- [6] Liu G.R., Liu M.B. *Smoothed Particle Hydrodynamics - a Meshfree Particle Method*, World Scientific Publ. 2007.
- [7] Manenti S., Ruol P., Fluid-Structure Interaction in Design of Offshore Wind Turbines: SPH Modeling of Basic Aspects, *Proc. Int. Workshop Handling Exception in Structural Engineering*, Nov. 13–14 2008, Sapienza University (Italy) DOI: 10.3267/HE2008.
- [8] Di Monaco A., Manenti S., Gallati M., Sibilla S., Agate G., Guandalini R., SPH modeling of solid boundaries through a semi-analytic approach. *J. Eng Appl. Comp. Fluid Mech.* Vol. 5, No. 1, pp. 1–15 (2011).
- [9] Manenti S., Agate G., Di Monaco A., Gallati M., Maffio A., Guandalini R., Sibilla S., SPH Modeling of Rapid Sediment Scour Induced by Water Flow. *33rd IAHR Cong.* August 9–14 2009 Vancouver, British Columbia (Canada).
- [10] Monaghan, J.J. Smoothed particle hydrodynamics, *Rep. Prog. Phys.* 68 1703–1759, (2005) doi:10.1088/0034-4885/68/8/R01.
- [11] Van Rijn L.C. Principles of sediment transport in rivers, estuaries, and coastal seas. *Aqua Publications* 1993 .
- [12] Cooper P.W. *Explosives Engineering*. Wiley-VCH, 1937.
- [13] Kedrinskii V.K. *Hydrodynamics of explosion – Experiments and models*. Springer, 2005.
- [14] Morris J.P., Fox P.J., Zhu Y. Modeling Low Reynolds Number Incompressible Flows Using SPH. *J. Comput. Phys.* 136, 214–226 (1997).
- [15] Kajtar J.B., Monaghan J.J. SPH simulations of swimming linked bodies. *J. Comput. Phys.* 227 (2008) 8568–8587.
- [16] Manenti S., Sibilla S., Gallati M., Agate G., Guandalini R. Prediction of Sediment Scouring through SPH. *Proc. 5th SPHERIC Int. Workshop* June 23-25 Manchester, Uk, pp. 56-60 2010.